# Cortical reactivity to transcranial magnetic stimulation predicts risk of post-stroke delirium

Yang Bai [a,b,c], Paolo Belardinelli [a,b,d], Catrina Thoennes [a,b], Corinna Blum [a,b], David Baur [a,b], Kornelia Laichinger [a,b], Tobias Lindig [e], Ulf Ziemann [a,b,*], Annerose Mengel [a,b]

[a] Department of Neurology & Stroke, University of Tübingen, Tübingen, Germany
[b] Hertie Institute for Clinical Brain Research, University of Tübingen, Tübingen, Germany
[c] School of Basic Medical Sciences, Hangzhou Normal University, Hangzhou, China
[d] Center for Mind/Brain Sciences - CIMeC, University of Trento, Italy
[e] Department of Neuroradiology, University of Tübingen, Tübingen, Germany

See Editorial, pages 95–96

## HIGHLIGHTS

- Low natural frequency and amplitude of TMS-EEG responses indicate high risk of post-stroke delirium (PSD).
- Low TMS-evoked connectivity indicate high risk of PSD.
- Low perturbation complexity index (PCI$^{ST}$) indicate high risk of PSD.

## ARTICLE INFO

## ABSTRACT

*Objective:* Post-stroke delirium (PSD) is a frequent and with regard to outcome unfavorable complication in acute stroke. The neurobiological mechanisms predisposing to PSD remain poorly understood, and biomarkers predicting its risk have not been established. We tested the hypothesis that hypoexcitable or disconnected brain networks predispose to PSD by measuring brain reactivity to transcranial magnetic stimulation with electroencephalography (TMS-EEG).
*Methods:* We conducted a cross-sectional study in 33 acute stroke patients within 48 hours of stroke onset. Brain reactivity to single-pulse TMS of dorsolateral prefrontal cortex, primary motor cortex and superior parietal lobule of the right hemisphere was quantified by response intensity, effective connectivity, perturbational complexity index (PCI$^{ST}$), and natural frequency of the TMS-EEG response. PSD development was clinically tracked every 8 hours before and for 7 days following TMS-EEG.
*Results:* Fourteen patients developed PSD while 19 patients did not. The PSD group showed lower excitability, effective connectivity, PCI$^{ST}$ and natural frequency compared to the non-PSD group. The maximum PCI$^{ST}$ over all three TMS sites demonstrated largest classification accuracy with a ROC-AUC of 0.943. This effect was independent of lesion size, affected hemisphere and stroke severity. Maximum PCI$^{ST}$ and maximum natural frequency correlated inversely with delirium duration.
*Conclusions:* Brain reactivity to TMS-EEG can unravel brain network states of reduced excitability, effective connectivity, perturbational complexity and natural frequency that identify acute stroke patients at high risk for development of delirium.
*Significance:* Findings provide novel insight into the pathophysiology of pre-delirium brain states and may promote effective delirium prevention strategies in those patients at high risk.

## 1. Introduction

Delirium is an acute neuropsychiatric complication, which results in a fluctuating disturbance in attention, awareness and

* Corresponding author at: Department of Neurology & Stroke, University of Tübingen, Hoppe-Seyler-Str. 3, 72076 Tübingen, Germany.
E-mail address: ulf.ziemann@uni-tuebingen.de (U. Ziemann).

cognition (American Psychiatric Association, 2013; Inouye et al., 2014), increases mortality, prolongs hospitalization and adversely affects functional outcomes following critical illness (Inouye et al., 1998; Khan et al., 2012; McCusker et al., 2002; Siddiq et al., 2006). Acute stroke is a known risk factor for the development of delirium (Gustafson et al., 1991; McManus et al., 2009). Although only limited published data on post-stroke delirium (PSD) exist, proportions of 10–27 % (Caeiro et al., 2004; Oldenbeuving et al., 2013) or higher (up to 48 %) (Dahl et al., 2010; Langhorne et al., 2000; Oldenbeuving et al., 2007) of PSD were indicated during the first critical weeks after stroke onset, making it a frequent and severe complication after stroke (Kiely et al., 2009; Shaw et al., 2019). Effective management, treatment and prevention of PSD may help to decrease incidence of mortality, disability (Rice et al., 2017; Song et al., 2018) and reduce clinical burden (Leslie et al., 2008; Maldonado, 2013). However, not much towards these aims has been achieved so far because detailed neural mechanisms underlying PSD are largely unclear, and markers to accurately predict PSD have not been developed.

Exploring the brain mechanisms underlying PSD will contribute to identifying patients who are at risk and aid clinicians in early initiation of delirium prevention and treatment. While the brain mechanisms of PSD are likely complex, several hypotheses from a molecular-biological perspective (Hshieh et al., 2008; van Munster et al., 2010) or an electrophysiological perspective (Wiegand et al., 2022) have been proposed to explain delirium development of mixed patient populations on the intensive care unit (ICU) (e.g., elderly patients post-surgery or with traumatic brain injury). In addition, neuroimaging studies highlighted altered functions of predominantly right-hemispheric cortical and subcortical networks for attention and arousal (Boukrina and Barrett, 2017) in delirium development. Still, the neurobiological basis and conditions involved in inducing a delirious brain state after stroke remain poorly understood.

Delirium prediction, which would facilitate early recognition of patients at high risk for delirium is, however, critical for clinical decision making and setting of priorities regarding the use of delirium preventive measures. In addition to usual precipitating factors for general ICU patients (van den Boogaard et al., 2014; Wassenaar et al., 2015), PSD is more likely to be dependent on stroke-related factors, such as stroke lesion location, lesion size, cerebral hypoperfusion and cerebral edema (Kostalova et al., 2012; Ojagbemi et al., 2017; Pasinska et al., 2018). Therefore, specialized neural assessment techniques (i.e., neurophysiology and neuroimaging) should be able to shed light on neural mechanisms underlying PSD and its prediction.

Transcranial magnetic stimulation (TMS)-EEG is a relatively novel technique, which provides a way for directly probing both local and widespread changes in brain neurophysiology, through the recording of TMS-evoked potentials and TMS-induced cortical oscillations. TMS-EEG can obtain important information regarding local excitability at the site of stimulation, and effective connectivity of both discrete and connected regions of the cortex, as well as providing insight into the oscillatory properties of brain networks (Tremblay et al., 2019). Compared to resting-state EEG, TMS-EEG enables direct and non-invasive exploration of cortical reactivity of the brain to external perturbation, with excellent temporal resolution. With regard to stroke patients, TMS-evoked brain responses were used to evaluate alterations in cortical reactivity (Sarasso et al., 2020), its reorganization (Pellicciari et al., 2018), and provided individual readout for prediction of motor recovery (Tscherpel et al., 2020).

Accordingly, we propose here that TMS-EEG-related neurophysiological markers of brain reactivity are capable of refining our understanding of the neurobiological basis of PSD. We hypothesize

that patients with reduced excitability and connectivity are at high-risk for development of PSD (Shafi et al., 2017).

## 2. Methods

### 2.1. Subjects

Thirty-three acute stroke patients (seventeen females; mean age ± SD: 78.4 ± 10.7 years, range: 52–93 years) (Table 1), who were admitted to the stroke unit of the department of Neurology & Stroke of the University Hospital Tübingen, were recruited into the study. Patients were enrolled based on the following inclusion criteria: (i) age >50 years in order to recruit a representative sample of stroke patients; (ii) acute ischemic or hemorrhagic stroke at supra- or infratentorial regions, verified by diffusion-weighted MRI (DWI); (iii) within the early acute stage, 48 hours after symptom onset; (iv) written informed consent obtained from the patients or their custodians prior to enrollment. Exclusion criteria were: (i) Richmond Agitation-Sedation Scale scores higher than 3 or lower than −4 at the time of the TMS-EEG measurement; (ii) PSD has already developed, or history of delirium, seizure or traumatic brain injury within the last three months; (iii) any contraindications to MRI or TMS (e.g., pacemakers, intracranial stents, epilepsy); (iv) central nervous system active drugs (e.g., benzodiazepines, neuroleptics) in the week prior to TMS-EEG measurement; (v) no detectable motor evoked potentials (MEP) in hand muscles with TMS of the primary motor cortex (M1) of either hemisphere, even at maximum stimulator output (MSO). The study was approved by the Ethics Committee of the University Hospital of Tübingen (protocol number 147/2020BO1).

### 2.2. PSD diagnosis

Delirium screening for the patients was conducted using the Intensive Care Delirium Screening Checklist (ICDSC), which was administered on admission and every 8 hours (morning, late and night shifts) for 7 days after the TMS-EEG measurement, by well-trained neurocritical care nurses. ICDSC scores of $\geq 4$ for non-aphasic, or $\geq 5$ for aphasic patients were considered indicative of PSD. Then, the diagnosis of PSD was confirmed in accord with the Diagnostic and Statistical Manual of the American Psychiatric Association (DSM-V) criteria by an independent neurologist, blinded for the ICDSC scores and TMS-EEG results. The delirium onset time, duration and end time were recorded (Table 1).

### 2.3. Data recording

#### 2.3.1. MRI data acquisition

High-resolution T1-weighted anatomical whole-brain volumes (3D MPRAGE, 176 sagittal slices, matrix size: 256 256; voxel size: 1 1 1 mm$^3$; TR: 1800 ms; TE: 2.5 ms; duration: 4 min 18 s) were obtained for all patients on a Siemens 3 Tesla Tim Trio scanner. Diffusion-weighted images (DWI) (TR = 3900 ms, TE = 95 ms, FOV = 230 mm, 22 axial slices, voxel size = 1.8 2.99 6 mm$^3$) were also acquired for all the patients in a clinical routine setting.

#### 2.3.2. TMS-EEG data recording and navigation

TMS-EEG data was acquired by a TMS-compatible EEG system (BrainAmp 64 actiCHamp Plus, BrainProducts GmbH, Munich, Germany). The EEG cap was equipped with TMS-compatible C-ring slit Ag/AgCl pin electrodes arranged in the International 10–20 montage. The EEG amplifier was set with a hardware filter at DC to 1 kHz and a sampling rate of 5 kHz. The skin/electrode impedances of all electrodes were maintained below 5 kΩ throughout the data

**Table 1**
Patient characteristics.

| Patients | Age/Gender | Lesion Side/ location | Lesion including cortical/subcortical regions | Lesion size (cm³) | Aphasia | NIHSS | RMT (% MSO) | Time (hours) of PSD onset after TMS-EEG/ICDSC | PSD duration (days) | Group (DSM-V) |
|---|---|---|---|---|---|---|---|---|---|---|
| 1 | 62/M | R/insula, internal capsule | Yes/Yes | 4.6 | No | 2 | 63 | – | – | non-PSD |
| 2 | 52/M | L/insula | Yes/No | 34.9 | Yes | 5 | 65 | – | – | non-PSD |
| 3 | 90/M | R/parietal, caudate nucleus | Yes/Yes | 142.6 | No | 4 | 66 | 24/6 | 2 | PSD |
| 4 | 57/M | R/thalamus | No/Yes | 0.5 | No | 3 | 55 | – | – | non-PSD |
| 5 | 89/F | R/insula, internal capsule | Yes/Yes | 13.7 | No | 6 | 55 | 156/6 | 1 | PSD |
| 6 | 76/F | R/insula | No/Yes | 5.7 | No | 0 | 48 | – | – | non-PSD |
| 7 | 80/M | L/parietal | Yes/No | 35.3 | No | 1 | 55 | – | – | non-PSD |
| 8 | 83/M | L/posterior cerebral artery, thalamus | Yes/Yes | 61.3 | No | 6 | 50 | 24/6 | 15 | PSD |
| 9 | 83/M | L/parietal, capsule | Yes/Yes | 134.0 | Yes | 20 | 56 | 16/5 | 6 | PSD |
| 10 | 80/F | R/insular | Yes/No | 1.4 | No | 12 | 65 | – | – | non-PSD |
| 11 | 68/F | L/basal ganglia | No/Yes | 1.0 | No | 1 | 55 | – | – | non-PSD |
| 12 | 75/F | R/temporal, internal capsule | Yes/Yes | 42.7 | No | 8 | 67 | 24/5 | 8 | PSD |
| 13 | 85/M | L/parietal | Yes/No | 0.5 | No | 0 | 57 | – | – | non-PSD |
| 14 | 89/F | R/parietal | Yes/Yes | 2.2 | No | 1 | 55 | – | – | non-PSD |
| 15 | 85/F | R/insula | Yes/Yes | 24.5 | No | 4 | 50 | – | – | non-PSD |
| 16 | 72/M | R/parietal | Yes/Yes | 34.6 | No | 0 | 45 | – | – | non-PSD |
| 17 | 80/F | L/insular | Yes/No | 72.4 | Yes | 7 | 75 | – | – | non-PSD |
| 18 | 83/M | R/parietal; L/insular | Yes/Yes | 13.5 | No | 3 | 57 | 32/7 | 15 | PSD |
| 19 | 93/F | R/capsular, insular | Yes/Yes | 40.1 | No | 3 | 44 | – | – | non-PSD |
| 20 | 58/M | R/frontal, caudate nucleus | Yes/Yes | 94.2 | No | 5 | #60 | 24/5 | 2 | PSD |
| 21 | 84/F | R/ caudate nucleus, superior temporal gyrus | No/Yes | 9.7 | No | 9 | 56 | 8/4 | 2 | PSD |
| 22 | 87/F | R/parietal | Yes/No | 16.3 | No | 12 | 48 | – | – | non-PSD |
| 23 | 69/F | R/posterior gyrus | Yes/No | 14.8 | No | 3 | 56 | – | – | non-PSD |
| 24 | 83/M | L/internal capsule, caudate nucleus | Yes/Yes | 45.7 | Yes | 15 | 44 | 8/4 | 2 | PSD |
| 25 | 90/F | L/parietal, motor | Yes/No | 30.9 | Yes | 18 | 60 | 16/4 | 3 | PSD |
| 26 | 69/M | R/posterior gyrus | Yes/Yes | 31.9 | No | 8 | 55 | 8/5 | 4 | PSD |
| 27 | 76/M | L/parietal, frontal, capsular | Yes/Yes | 47.2 | Yes | 17 | 48 | 8/5 | 2 | PSD |
| 28 | 83/F | L/capsular | No/Yes | 19.1 | Yes | 18 | 49 | 24/5 | 2 | PSD |
| 29 | 87/F | L/longitudinal fasciculus | Yes/Yes | 0.1 | No | 0 | 45 | – | – | non-PSD |
| 30 | 70/M | R/temporal gyrus, capsular | Yes/Yes | 42.9 | No | 12 | 60 | – | – | non-PSD |
| 31 | 83/M | L/insular, capsular | Yes/Yes | 20.5 | Yes | 3 | 45 | – | – | non-PSD |
| 32 | 89/F | R/parietal | Yes/No | 19.6 | No | 5 | #55 | – | – | non-PSD |
| 33 | 89/F | R/parietal | Yes/Yes | 2.8 | No | 4 | #50 | 16/5 | 3 | PSD |

F: female; M: male; R: right hemisphere; L: left hemisphere; NIHSS: National Institutes of Health Stroke Scale; RMT: resting motor threshold; MSO: maximum stimulator output; #: RMT was determined in the left hemispheric M1; ICDSC: Intensive Care Delirium Screening Checklist; DSM-V: Diagnostic and Statistical Manual of American Psychiatric Association; PSD: post-stroke delirium; non-PSD: post-stroke without delirium; TMS-EEG: transcranial magnetic stimulation – electroencephalography.

recordings. TMS pulses were delivered through a MagVenture (MagPro Compact, MagVenture A/S, Denmark) magnetic stimulator with a monophasic current waveform. A stereoscopic neuronavigation system (Localite GmbH, St. Augustin, Germany) was used, based on individual anatomical MRI to enable precise positioning of the TMS coil relative to the individual brain anatomy. To define the standardized localization of the TMS targets, the individual brains were projected to a template according to the Montreal Neurological Institute (MNI) coordinate system based on the anatomical positions of the anterior commissure, posterior commissure and one point on the falx cerebri.

Prior to the TMS-EEG recordings, the individual resting motor threshold (RMT) in the right M1 was determined by MEP recordings (Tscherpel et al., 2020) (see details in Supplementary Materials). RMT of 3 patients (Table 1) was determined in the left hemispheric M1, since no MEP could be elicited from the right M1, even with TMS intensity of 100 % MSO. The RMT in the PSD (mean 1SD: 54.8 8.3 % MSO) vs non-PSD group (mean 1SD: 55.2 6.7 % MSO) was not different ($p > 0.05$, independent two-sample $t$-test).

Right-hemispheric cortical regions, including dorsolateral prefrontal cortex (DLPFC), primary motor cortex (M1) and superior parietal lobule (SPL) were shown to have a close association with delirium (Boukrina and Barrett, 2017). Accordingly, three right-hemispheric TMS targets were defined and set at the individually MNI-fitted images according to the MNI coordinates (DLPFC: $x = 38$, $y = 19$, $z = 51$; M1: $x = 51$, $y = -8$, $z = 44$; SPL: $x = 19$,

$y = -54$, $z = 64$; marked as red dots in Fig. 1 A–C) to make stimulation sites comparable between patients. Importantly, the individual target sites were evaluated prior to each TMS measurement by a neurologist according to the individual DWI information on the ischemic stroke lesion. The individual target sites close (<2 cm) to lesions (M1 in one non-PSD and one PSD patient, DLPFC in one non-PSD patient) were skipped in order to avoid impact on our findings from perilesional cortical off-periods (Sarasso et al., 2020) or inexcitable cortex (Gosseries et al., 2015).

During the TMS-EEG recordings, single-pulse TMS at an intensity of 90 % RMT was delivered at the three targets in separate blocks of 200 trials, with jittered inter-trial intervals of on average 2 s. The order of the targets was pseudo-randomized and balanced across patients. TMS coil was set and optimized at each target under online neuronavigation to induce an electric field perpendicular to the main axis of the targeted gyrus. To investigate whether
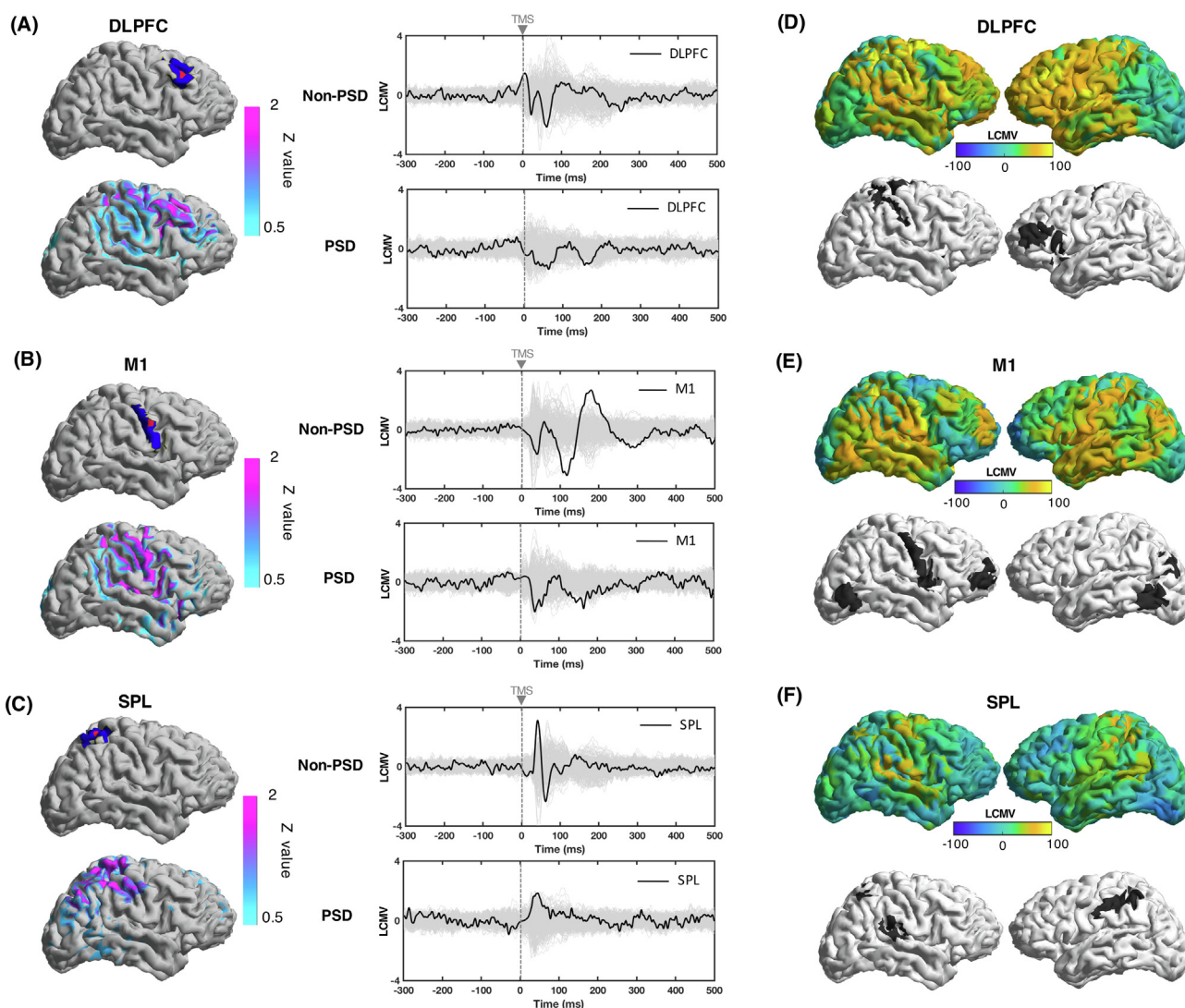


**Fig. 1.** Cortical responses evoked by transcranial magnetic stimulation (TMS) in dorsolateral prefrontal cortex (DLPFC), primary motor cortex (M1) and superior parietal lobule (SPL). (A–C) Left column shows TMS target regions of DLPFC, M1 and SPL in the Brainnetome Atlas (dark blue) and navigated TMS target sites (red dots). Spatial distribution plots represent average cortical activity of all patients (absolute z-transformation relative to the baseline [−300 ms −50 ms]) elicited over the first 100 ms after the TMS pulse. Butterfly plots: group average cortical reactivity (y-axes: linearly constrained minimum variance (LCMV) values) evoked by TMS (time, 0 ms) of DLPFC (A), M1 (B) and SPL (C) of non-post-stroke delirium (non-PSD) group (upper plots) and the PSD group (lower plots). The black traces indicate TMS evoked response in the target regions underneath the TMS coil (defined as dark blue in the left column). The response intensity was defined as summarized absolute values of significant (bootstrap nonparametric statistics with $p < 0.01$) cortical responses between 20 ms to 300 ms. Each gray trace indicates a TMS evoked responses from one brain region. Spatial activation maps show the difference of cortical response intensity between non-PSD and PSD groups evoked by TMS of DLPFC (D), M1 (E) and SPL (F). Yellow colors indicate higher values in the non-PSD group. Black colors in the underneath cortex plots show regions with significant difference (Mann-Whitney *U*-test, FDR correction with $p < 0.05$) of response intensity between non-PSD vs PSD groups.

the stimulation intensity was comparable within and between patients, distribution and intensity of the intracranial electric field induced by TMS were calculated at each target site of each patient using the SimNIBS toolbox (Saturnino et al., 2019). The mean (±1SD) strengths of the electric fields were calculated at the defined targets and compared between non-PSD vs PSD groups. Importantly, there were no significant group differences (non-PSD vs PSD): 99.8 ± 17.2 V/m vs 100.1 ± 12.6 V/m at DLPFC, 91.4 ± 13.7 V/m vs 96.6 ± 15.4 V/m at M1, 81.6 ± 12.7 V/m vs 85.9 ± 14.5 V/m at SPL, and all individual electrical field strengths were sufficient (>40 V/m) to evoke distinct cortical reactivity (Rosanova et al., 2009). The methodological details are given in the Supplementary Materials (Figure S5 and related content).

Although noise masking is always suggested, long-time exposure with high-decibel (up to 90 dB) white noise turned out to be intolerable for most of the acute stroke patients, and might even constitute a risk factor for inducing delirium (Kalish et al., 2014). Therefore, we chose earplugs but not noise masking during TMS-EEG recording. Before performing further analysis on TMS-EEG, we investigated the cortical response elicited by the TMS clicks, which is represented by a wave component in the central region between 100–200 ms (Rocchi et al., 2021). We extracted the cortical auditory evoked potential (AEP, N1: 80–120 ms and P2: 160–200 ms) by averaging the TMS evoked potentials recorded over FCz and the eight surrounding electrodes (F1, Fz, F2, FC1, FC2, C1, Cz and C2) (Vallesi et al., 2021). The N1 (80–120 ms following the TMS pulses) and P2 (160–200 ms) components of the AEP and their topographies with TMS of DLPFC, M1 and SPL are shown in Supplementary Material (Figure S6). N1 and P2 were reconstructed in source space. Cortical areas of interests for cortical AEP analysis, including Heschl's gyrus, Brodmann area 22 and planum temporale, were identified in MNI coordinates, in accord with previous AEP localizing studies (Gascoyne et al., 2016; Godey et al., 2001) and mapped onto the Brainnetome Atlas (Supplementary Materials, Figure S7A). Then, the absolute values of cortical AEP amplitudes in these cortical areas of interests were reconstructed for each patient using a linearly constrained minimum variance (LCMV) beamforming method (Sekihara and Nagarajan, 2008). The AEP-related cortical responses were extracted, by averaging values in the areas of interests, within the period 80–120 ms for N1, and 160–200 ms for P2.

## 2.4. Data analysis

Preprocessing of TMS-EEG (Rogasch et al., 2014) were performed using customized analysis scripts on MATLAB (Version 2017b, MathWorks Inc., Natick, USA) and EEGLAB 14.1.2b. A LCMV beamforming method (Sekihara and Nagarajan, 2008) was used to perform source reconstruction based on the FieldTrip toolbox and FreeSurfer (see methodology details of data preprocessing and source reconstruction in Supplementary Materials).

### 2.4.1. TMS evoked potentials (TEPs)

To estimate the neuronal responses elicited by TMS, we projected the source-reconstructed responses into the human Brainnetome Atlas (Fan et al., 2016) containing 246 regions of interest (ROIs) across both hemispheres. The activity for each of these ROIs was estimated by taking the first component from a principal component analysis performed on the time course of dipoles included in the ROIs. Based on the Atlas, we defined the DLPFC, M1 and SPL, according to their spatial positions (marked as dark blue areas in Fig. 1A-C). In order to validate the accuracy of the navigation procedure and support the choice of the ROIs, we estimated the intensity distribution of the neuronal responses elicited by TMS. The neuronal response of each dipole after source reconstruction was firstly normalized by z-transformation relative to the baseline

(−300 ms to −20 ms) and then averaged over the first 100 ms (21 ms to 100 ms, first 20 ms discarded in order to avoid possible non-neuronal activities) after TMS.

### 2.4.2. Effective connectivity

TMS evoked effective connectivity was measured by detecting directional information flow elicited (time-locking) by the TMS pulse. Symbolic transfer entropy was calculated in pairs of TEPs (21 ms to 400 ms) of ROIs with recommended parameter settings (number of symbols: 4, step interval: 16 ms, forward step: 50 ms) (Ye et al., 2020). A bootstrap procedure was conducted to exclude spurious connectivity in each individual. It generated 1000 surrogating information flow matrices by calculating symbolic transfer entropy on shuffled TEPs. The connectivity strength was set to zero if they did not exceed 95 % of surrogating strength.

### 2.4.3. Perturbational complexity index (PCI$^{ST}$) and natural frequencies

We measured the cortical reactivity evoked (i.e., phase-locked, TEPs) and induced (i.e., non-phase-locked, time–frequency representations, TFRs) by TMS. The PCI$^{ST}$ measures the ability of the whole cortex to engage in complex patterns of causal interactions by quantifying the non-redundant state transitions across all principal components of the evoked perturbation signals (Comolatti et al., 2019). The PCI$^{ST}$ values were calculated on averaged source-reconstructed TEPs of each patient, and group averaged source-reconstructed TEPs of PSD and non-PSD groups, separately for TMS of each target site (DLPFC, M1 and SPL). The principal components were selected so as to account for at least 99 % of variance of the response amplitude, and components with low signal-to-noise ratio (SNR ≤ 1.1) were removed. The average number of state transitions in the matrices of the response (20 ms to 300 ms) was compared with that of the baseline (−300 ms to −20 ms). A parameter k (set to 1.2 in this study) was used to control the relative weight of state transitions between baseline and response. More details of the computing pipeline and additional results of TEPs and PCI$^{ST}$ at the sensor level are given in the Supplementary Materials (Figures S2-S3 and related content).

To explore the oscillatory information induced by TMS, we performed event-related spectral perturbation (ERSP) analysis. The induced neuronal responses were isolated by subtracting the individual time-domain average from each trial (Cohen and Donner, 2013). Time-frequency representations (TFRs) of TMS-related oscillatory power were calculated, separately for each ROI at the single trial level, by means of a Hanning taper windowed FFT with frequency dependent window length (width: 3.5 cycles per time window, time steps: 10 ms, frequency steps: 0.25 Hz from 4 to 45 Hz). Data from −1000 ms to 1000 ms around the TMS pulse was selected to ensure a sufficient time and frequency resolution of the ERSPs. We performed single-trial normalization by z-transforming the TFRs and baseline correction (subtracting the average of the −300 ms to −20 ms period) of each trial for each frequency (Premoli et al., 2017). Then, the ERSPs were extracted by cropping the TFRs during the time of interest (−100 ms to 400 ms) for further statistical analysis.

Natural frequency of each ROI was assessed by estimating the main frequency of the local TMS-induced oscillations. We calculated the power spectrum profiles by averaging the oscillatory power between 21 ms to 400 ms of the ERSPs at each target ROI. Then the natural frequency was defined corresponding to the maximum peak of the power spectrum profile (Rosanova et al., 2009; Tscherpel et al., 2020).

### 2.4.4. Lesion maps

Individual lesion maps were manually created and cross-validated by three well-trained physicians on DWI images through the software MRIcron (https://www.nitrc.org/projects/mricron).

Then, the individual lesion maps and DWI images were co-registered to the individual T1-weighted images by Statistical Parametric Mapping (SPM12, https://www.fil.ion.ucl.ac.uk/spm/software/spm12/). Lesion size was measured by the number of damaged voxels. To investigate possible associations between specific damaged voxels and development of PSD, we normalized the individual T1-weighted images and lesion maps to the T1-weighted MNI-template implemented in SPM12.

### 2.5. Data availability

The data that support the findings of this study and all custom written MATLAB codes are available from the corresponding author upon reasonable request.

### 2.6. Statistics

Bootstrap sampling statistics was used to determine significant cortical responses (Casali et al., 2013). Brain excitability was determined as the summed absolute values of significant cortical responses (TEPs) between 20 ms to 300 ms. Excitability of brain regions (defined by the Brainnetome Atlas) was compared between PSD vs non-PSD groups by non-parametric Mann-Whitney $U$-tests and FDR correction with $p < 0.05$. We conducted non-parametric permutation tests ($p < 0.05$) to indicate significantly different information flow matrix between PSD and non-PSD groups. Information sending/receiving of ROIs were summarized from rows/columns of information flow matrix in each individual. ROIs with significantly different information sending/receiving between PSD and non-PSD groups were detected by Mann-Whitney $U$-test and FDR correction with $p < 0.05$.

Two-way repeated measures analyses of variance (rmANOVAs) were conducted for the cortical AEP components N1 and P2 in source space, with the repeated effect of TMS target (3 levels: DLPFC, M1 and SPL) and the effect of group (2 levels: non-PSD and PSD), after verification that the data were normally distributed. Post-hoc independent-sample two-tailed $t$-tests were performed in case of a significant effect of group, or interaction of group with TMS target, to compare non-PSD vs PSD. $P$ values were Bonferroni-corrected for multiple comparisons.

To compare cortical reactivity (PCI$^{ST}$ and natural frequency) between PSD and non-PSD groups, we conducted a two-way rmANOVA using the software SPSS (version 25), after verifying normal distribution of all data. Repeated effect of TMS target (3 levels: DLPFC, M1 and SPL) and effect of group (2 levels: non-PSD and PSD) were investigated. Post-hoc independent-sample two-tailed $t$-tests were performed in case of a significant effect of group to compare the PSD vs non-PSD group. $P$ values after multiple comparisons were adjusted using Bonferroni correction. Non-parametric Mann-Whitney $U$-test was performed to compare lesion size between PSD and non-PSD group, since lesion size did not follow a normal distribution. Receiver operating characteristic curve (ROC) and area under ROC (AUC) were used to assess classification ability of TMS-EEG characteristics and lesion size in distinguishing PSD vs non-PSD.

Relationships of maximum values of PCI$^{ST}$ and natural frequency with delirium duration were tested by Pearson correlation analyses and simple linear regressions with scatter-plots. In order to investigate the associations between specific stroke-affected voxels and delirium and TMS-EEG characteristics, we conducted a voxel lesion symptom mapping (VLSM) analysis. Based on normalized T1-weighted lesion maps, voxels that were damaged in at least two patients in either group were included for statistical analysis (Tscherpel et al., 2020). VLSM was calculated with the NiiStat software (https://github.com/neurolabusc/NiiStat) running on the MATLAB environment and displayed on a T1-weighted

MNI-template head by MRIcroGL. Non-parametric permutation tests (2000 permutations) were used to correct for multiple comparisons.

We performed a stepwise logistic regression analysis and a Wald statistic to investigate the strongest predictor of risk of delirium among all the neurophysiologic, imaging and clinical markers, including PCI$^{ST}$ and natural frequency obtained at each of the three TMS targets, maximum PCI$^{ST}$ and maximum natural frequency across the three TMS target sites, and lesion size and NIHSS score.

## 3. Results

Fourteen patients (8 males, 6 females; mean ± 1SD age, 81.1 ± 9.0 years) developed delirium after the TMS-EEG measurement (range of onset after the TMS-EEG measurement, 8–156 hrs according to longitudinal ICDSC assessment), and were defined as the PSD group (DSM-V). Nineteen patients (8 males, 11 females; mean ± 1SD age, 77.1 ± 11.6 years), who did not develop delirium over the 7 days following the TMS-EEG measurement, were defined as the non-PSD group (Table 1).

### 3.1. TMS-evoked potentials (TEPs)

The TMS-evoked EEG responses (absolute z-values relative to the baseline, averaged over all patients, in a window 21 – 100 ms after the TMS pulse) occurred mainly at the site of the TMS targets (red dots indicate neuronavigated targets in DLPFC, M1 and SPL) and ROIs (dark blue areas) defined by the Brainnetome Atlas (Fig. 1A-C). This verifies that the intended cortical TMS targets were successfully activated.

Temporal and spatial characteristics of TEPs of DLPFC (Fig. 1A), M1 (Fig. 1B) and SPL (Fig. 1C) were different in the PSD vs non-PSD group averages. The spatial activation maps of TMS-evoked response intensity (absolute sum of significant responses 20 – 300 ms post-stimulus, bootstrap non-parametric statistics with 1000 times shuffling) showed widely decreased cortical responses in PSD compared to non-PSD group. The significantly decreased responses (non-parametric Mann-Whitney $U$-test, FDR corrected with $p < 0.05$) involved, in addition to local activation, several cortical sources distant from the stimulated sites (Fig. 1D–F).

Cortical AEP amplitudes showed significant interactions between TMS target and group for N1 ($F_{(1,94)} = 125.8$, $p < 0.001$) and P2 ($F_{(1,94)} = 93.3$, $p < 0.001$) but, importantly, post-hoc $t$-tests did not reveal any significant differences of N1 or P2 between the PSD vs non-PSD groups for any of the three TMS targets (Supplementary Materials, Figure S7B).

### 3.2. Effective connectivity

TMS evoked effective connectivity was significantly decreased in PSD compared to non-PSD (non-parametric permutation tests, $p < 0.05$), particularly when TMS targeted DLPFC and M1 (Fig. 2-A-C). This decrease in effective connectivity in PSD was mainly caused by a significant decrease of receiving information in distributed brain regions (Mann-Whitney $U$-test, FDR correction with $p < 0.05$) rather than a decrease in sending information (Fig. 2A-C).

### 3.3. Perturbational complexity index

The PCI$^{ST}$ values (including data of all three TMS targets) of the PSD group (mean ± 1SD: 52.3 ± 12.3) were significantly lower ($p < 0.001$, $t = -7.3$, independent two-sample $t$-test) than the values of the non-PSD group (mean ± 1SD: 73.7 ± 15.5) (Fig. 3A). Two-way rmANOVA revealed a significant effect of group, with lower PCI$^{ST}$ values in the PSD group compared to the non-PSD group [main
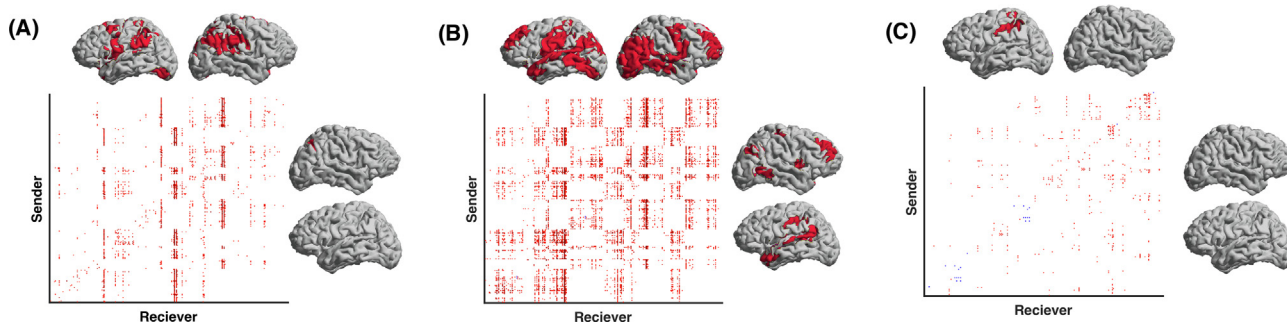
**Fig. 2.** Transcranial magnetic stimulation (TMS) evoked connectivity in dorsolateral prefrontal cortex (DLPFC), primary motor cortex (M1) and superior parietal lobule (SPL). (A–C) TMS evoked information flow matrix with significantly different (permutation tests, level of statistical significance, $p < 0.05$) symbolic transfer entropy values between the post-stroke delirium (PSD) and non-PSD group, with TMS targeting DLPFC (D), M1 (E) and SPL (F). Red indicates lower value in PSD and blue indicates higher value in PSD. Cortex plots show regions sending (right of the matrix) and receiving information (above the matrix), which was significantly weaker (Mann-Whitney $U$-test, FDR correction with $p < 0.05$) in PSD than non-PSD group.
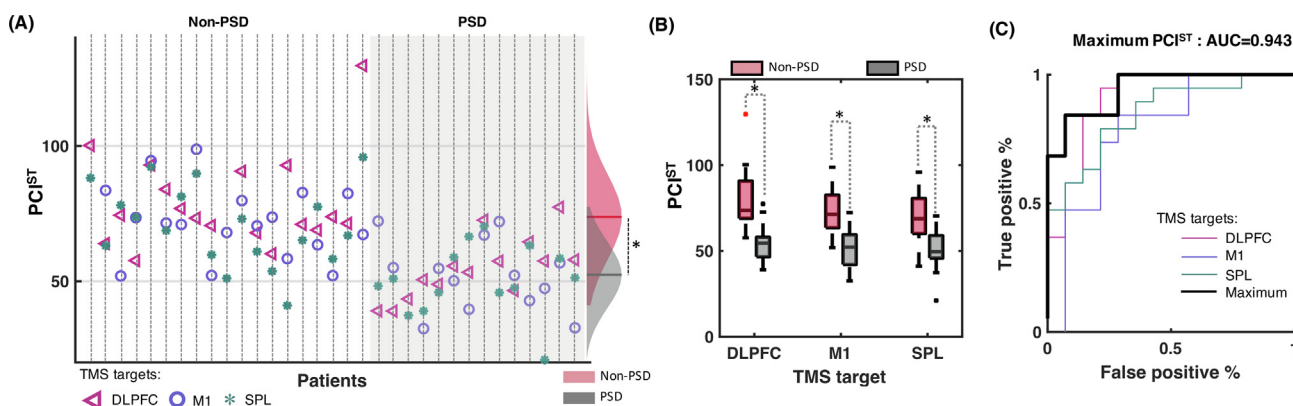


**Fig. 3.** Perturbational complexity index ($PCI^{ST}$) values in 33 stroke patients obtained with transcranial magnetic stimulation with electroencephalography (TMS-EEG) of three brain areas. (A) Scatter plot of individual $PCI^{ST}$ values obtained with TMS of dorsolateral prefrontal cortex (DLPFC, pink triangles), primary motor cortex (M1, purple circles) and superior parietal lobule (SPL, green asterisks). Each vertical dotted line represents values coming from one patient. Gray area indicates patients who developed post-stroke delirium (PSD) while white area indicates patients who did not develop delirium (non-PSD). Right part of the panel displays Gaussian distributions and statistics (independent two-sample $t$-test, * $p < 0.001$) of $PCI^{ST}$ values in the non-PSD (red) and PSD (gray) groups, where horizontal lines represent group averages. (B) Boxplots of $PCI^{ST}$ values obtained with TMS of DLPFC, M1 and SPL divided into non-PSD (red) and PSD (gray) group (* indicates significance after Bonferroni correction, all $p < 0.001$; two-way rmANOVA with post-hoc independent two-sample $t$-tests). (C) Receiver operating characteristic curves of $PCI^{ST}$ values obtained with TMS of DLPFC, M1 and SPL as well as maximum $PCI^{ST}$ across the three TMS sites in classification of non-PSD vs PSD groups. Area under the curve (AUC) of the maximum $PCI^{ST}$ is indicated.

effect of group: $F_{(1,90)} = 54.4$, $p < 0.001$], without significant interaction with TMS target [$F_{(2,90)} = 2.4$, $p > 0.05$]. Post hoc $t$-tests disclosed a between group difference with significantly lower $PCI^{ST}$ values in the PSD group compared to the non-PSD group for each of the three TMS targets (mean ± 1SD of PSD vs non-PSD at DLPFC: 52.3 ± 12.3 vs 78.9 ± 17.3; at M1: 52.0 ± 13.2 vs 72.0 ± 13.6; at SPL: 50.3 ± 13.0 vs 70.4 ± 14.9) (all $p < 0.001$) (Fig. 3B). The $PCI^{ST}$ values with TMS of either DLPFC (AUC = 0.910), M1 (AUC = 0.790) or SPL (AUC = 0.850) could effectively distinguish between PSD and non-PSD (Fig. 3C). When taking the maximum $PCI^{ST}$ across the three TMS targets in each patient, the classification reached an AUC of 0.943 (Fig. 3C), higher than the AUCs of resting-state power spectral density analyses (Figure S1 and related content in Supplementary Materials). In addition, these $PCI^{ST}$ data analyzed at source level were validated by a $PCI^{ST}$ analysis at sensor level that provided virtually identical findings (Figures S2-S3 and related content in Supplementary Materials).

### 3.4. Natural frequencies

Two-way rmANOVA indicated a significant difference with lower natural frequencies in the PSD compared to non-PSD group [mean ± 1SD of PSD vs non-PSD: 9.9 ± 5.8 Hz vs 14.5 ± 7.4 Hz; main effect of group: $F_{(1,90)} = 11.1$, $p = 0.001$], without interaction with

TMS target [$F_{(2,90)} = 2.7$, $p = 0.075$]. When comparing the natural frequency between PSD and non-PSD groups at each target, the post hoc $t$-tests revealed significantly lower natural frequency of PSD than non-PSD at DLPFC (mean ± 1SD of PSD vs non-PSD: 9.5 ± 4.8 Hz vs 15.6 ± 7.1 Hz) (Fig. 4A) and SPL (9.8 ± 5.6 Hz vs 17.1 ± 7.5 Hz) (Fig. 4C) but not at M1 (10.5 ± 7.3 Hz vs 10.7 ± 6.3 Hz) (Fig. 4B).

### 3.5. Relationship between stroke lesions, stroke severity, cortical reactivity and delirium

The lesion size in the PSD group (mean ± 1SD: 49.2 ± 44.7 cm³) was significantly larger ($U = 59$, $p = 0.028$, Mann-Whitney-$U$-test) than in the non-PSD group (mean ± 1SD: 19.6 ± 20.9 cm³) (Fig. 5A). Pearson correlation indicated that lesion size had significant inverse correlations with $PCI^{ST}$ at DLPFC ($r = -0.50$, $p = 0.006$) and SPL ($r = -0.440$, $p = 0.015$) (Fig. 5B-C) but not with $PCI^{ST}$ at M1.

The NIHSS score in the PSD group (mean ± 1SD: 9.9 ± 6.2) was significantly higher ($U = 309$, $p < 0.001$, Mann-Whitney-$U$-test) than in the non-PSD group (mean ± 1SD: 3.6 ± 4.3) (Fig. 5D). NIHSS scores were significantly inversely correlated with $PCI^{ST}$ values at M1 ($r = -0.459$, $p = 0.012$) and SPL ($r = -0.645$, $p < 0.001$) (Fig. 5E–F) but not with $PCI^{ST}$ at DLPFC.
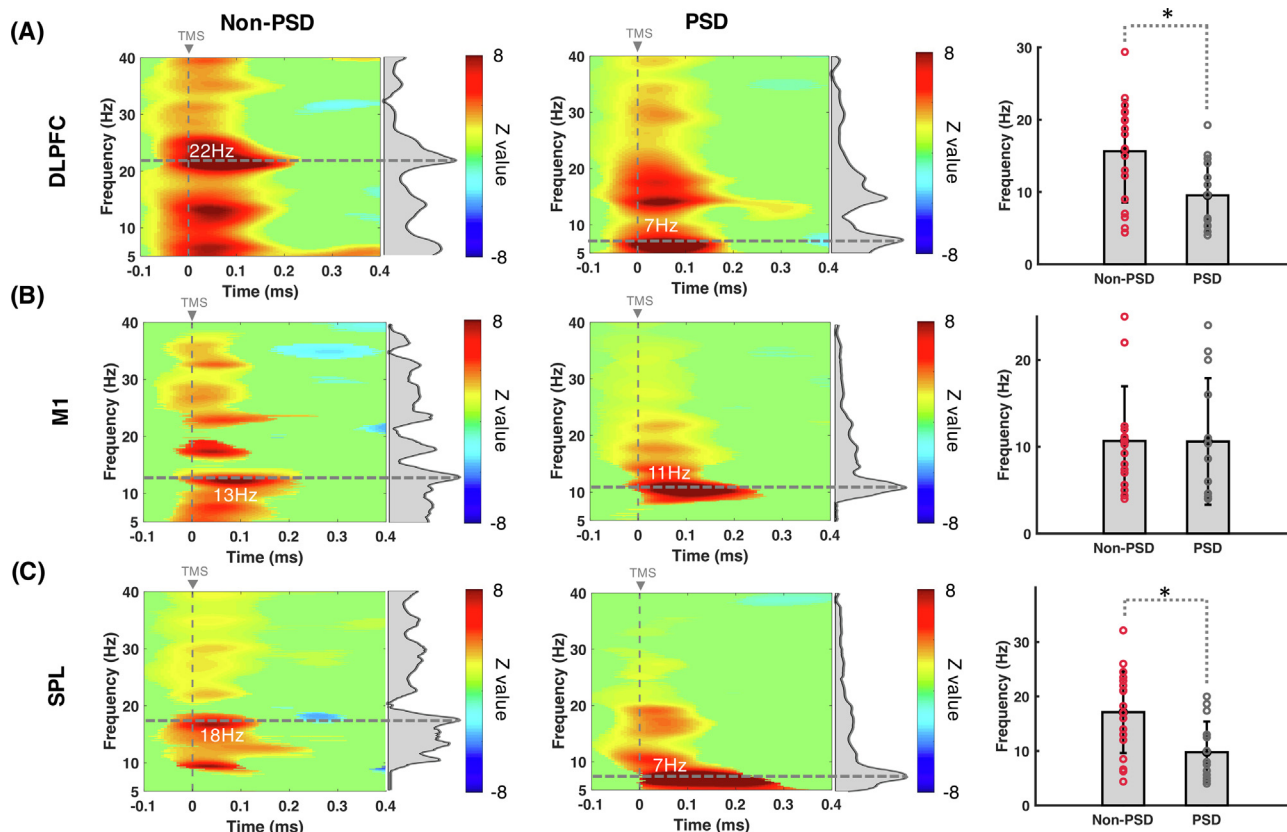
**Fig. 4.** Event-Related Spectral Perturbations (ERSPs) and natural frequencies. The time–frequency plots show the TMS-related ERSPs extracted from the stimulated areas, (A) dorsolateral prefrontal cortex (DLPFC), (B) primary motor cortex (M1), and (C) superior parietal lobule (SPL), of one representative patient with non-post-stroke delirium (non-PSD) (left column) and another patient with PSD (middle column). The gray area plotted at the right of each time–frequency plot depicts the power spectrum profile elicited during the first 400 ms after transcranial magnetic stimulation (TMS). The horizontal dashed lines highlight maximum power corresponding to the natural frequency (indicated in Hz also in the time–frequency plots). Right panel shows individual natural frequencies (means 1SD) at DLPFC, M1 and SPL. * indicate statistical significance (two-way rmANOVA with post-hoc independent two-sample *t*-tests, Bonferroni-corrected for multiple comparisons) between non-PSD (red circles) and PSD (gray circles) groups.

Lesion size (AUC = 0.737) or NIHSS (AUC = 0.852) alone did not achieve better classification between PSD and non-PSD than TMS-EEG characteristics. Furthermore, the Bayesian analysis of covariance (Supplementary Materials, Figure S4) did not provide evidence for the inclusion of the stroke-affected hemisphere as a significant factor in predicting post-stroke delirium in conjunction with $PCI^{ST}$ or natural frequency.

VLSM analysis revealed that the $PCI^{ST}$ at SPL was associated with small lesion clusters in the subcortical white matter of the corona radiata (Fig. 6A). Natural frequency at DLPFC was associated with small lesion clusters in frontal cortex (Fig. 6B).

A stepwise logistic regression analysis indicated that the strongest predictor (Chi2Stat = 26.08, $p < 0.001$) of delirium risk was maximum $PCI^{ST}$. Its predictive effect was confirmed by Wald statistic (Wald statistic = 6.16, $p = 0.013$) (Fig. 6C). The Wald statistic indicated that only NIHSS score (Wald statistic = 4.13, $p = 0.042$) potentially contributed to the predictive model of maximum $PCI^{ST}$.

The maximum $PCI^{ST}$ value ($r = -0.56$, $p = 0.039$) (Fig. 6D) and the maximum natural frequency ($r = -0.56$, $p = 0.037$) (Fig. 6E) across the three TMS target sites (DLPFC, M1 and SPL) were significantly inversely correlated with delirium duration.

## 4. Discussion

EEG and functional MRI research have verified that delirium is a disconnection syndrome, i.e., a consequence of a breakdown of connectivity in brain networks (Sanders, 2011; van Dellen et al.,

2014). Thus, measuring connectivity of brain networks will be a more direct approach to probe the underlying mechanism of delirium, and possibly provide the opportunity to predict delirium prior to its onset (Shafi et al., 2017). However, resting-state EEG and fMRI passively record brain activity and, therefore, are limited in their capacity to make inferences about brain function. In contrast, TMS-EEG provides a powerful means to directly measure the cerebral response to a defined perturbation, which allows testing of effective connectivity. Although preliminary, our study indicates, to the best of our knowledge for the first time, that TMS-EEG can be used to predict the risk of PSD. We present evidence that abnormalities of cortical reactivity to TMS, quantified by evoked responses, evoked connectivity and induced oscillations, are associated with the risk of delirium development during the following days. Specifically, those acute stroke patients, who presented with low maximum $PCI^{ST}$, had a high risk of PSD.

TEPs reflect spatial and temporal summation of excitatory and inhibitory post-synaptic potentials, time-locked to the TMS pulse, and originating from the activity of a large population of cortical pyramidal neurons and interneurons (Hill et al., 2016). Abnormal TEP morphologies are linked with altered brain states caused by, e.g., severe psychiatric or neurological disorders (Tremblay et al., 2019). A high-amplitude and low-complexity early component was demonstrated as the TEP characteristic in stroke patients (Sarasso et al., 2020), and was associated with severity of initial neurological deficit and functional outcome at 90-day follow-up (Tscherpel et al., 2020). The present study revealed that PSD patients exhibited TEPs with reduced amplitude and number of
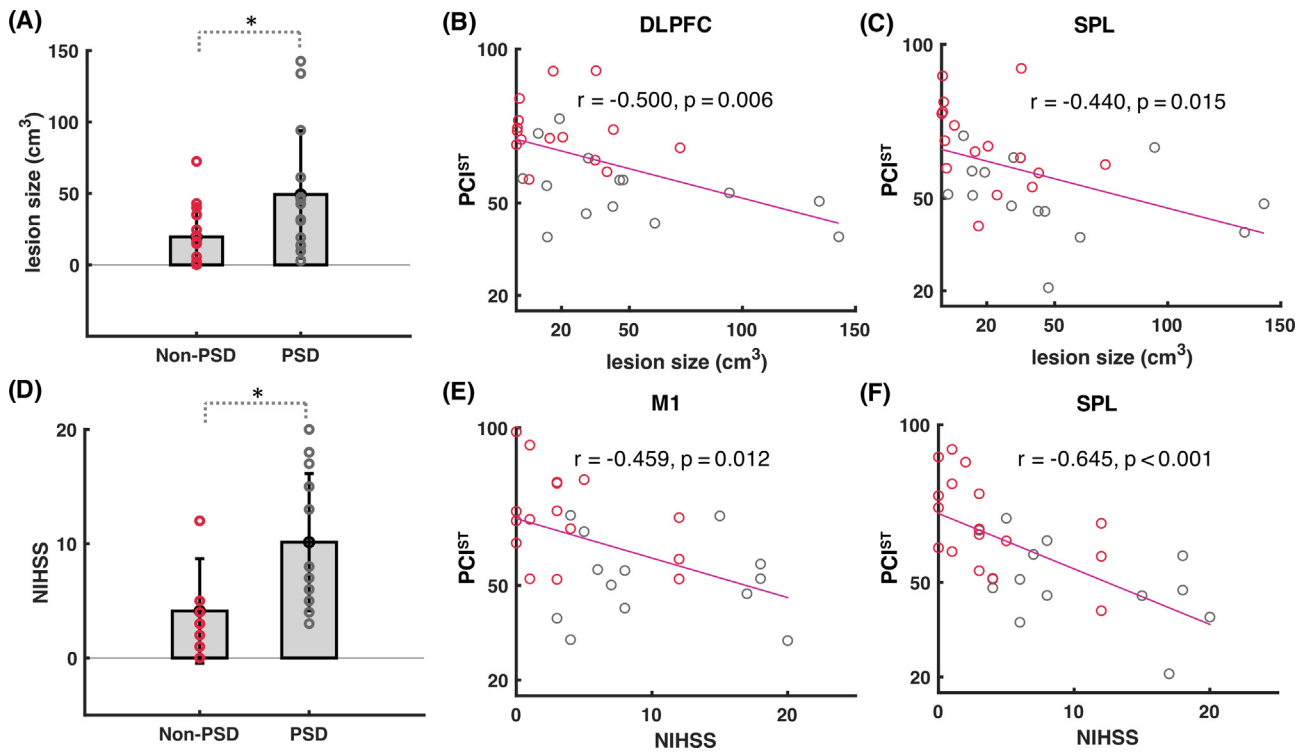
**Fig. 5.** Relationship of lesion size and stroke severity with cortical reactivity. (A) Individual lesion size (means 1SD) in the non-post-stroke delirium (non-PSD, red circles) vs PSD (gray circles) group (* indicates $p < 0.05$, Mann-Whitney-$U$-test). (B-C) Plots of perturbational complexity index (PCI$^{ST}$) values obtained with (B) transcranial magnetic stimulation (TMS) of dorsolateral prefrontal cortex (DLPFC) or (C) superior parietal lobule (SPL) as a function of stroke lesion size. (D) National Institutes of Health Stroke Scale (NIHSS) as index of stroke severity at the time of the measurements (means 1SD) in the non-PSD (red circles) vs PSD (gray circles) group (* indicates $p < 0.001$, Mann-Whitney-$U$-test). (E–F) Plots of PCI$^{ST}$ values obtained with (E) TMS of primary motor cortex (M1) or (F) SPL as a function of NIHSS. Red circles show non-PSD patients and gray circles PSD patients. Regression lines and Pearson correlations with correlation coefficients ($r$) and $p$ values are indicated.
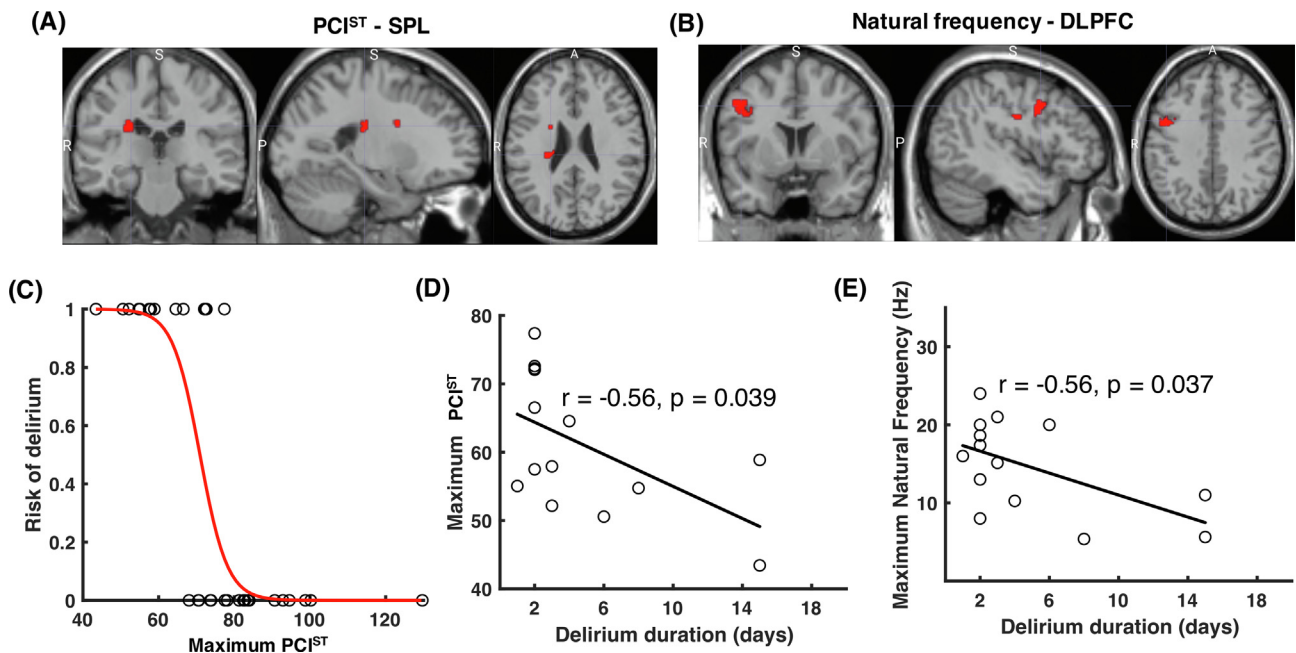


**Fig. 6.** Relationship of cortical reactivity with stroke lesions and delirium duration. (A-B) Red color highlights lesion voxel clusters related to the perturbational complexity index (PCI$^{ST}$) obtained with transcranial magnetic stimulation (TMS) of superior parietal lobule (SPL) (A) and natural frequency at dorsolateral prefrontal cortex (DLPFC) (B). Comparisons were performed by voxel lesion symptom mapping and non-parametric permutation tests. Only voxel clusters >10 mm$^3$ are displayed. A = anterior; P = posterior; R = right; S = superior. (C) Observed values (each circle corresponds to one stroke patient) indicating post-stroke delirium development (y = 1) or not (y = 0) against maximum PCI$^{ST}$. The red line represents the estimated logistic regression curve between the predicted risk of delirium development and the maximum PCI$^{ST}$ values. Scatter plots and Pearson correlations of maximum PCI$^{ST}$ values (D) and maximum natural frequency (E), as a function of delirium duration. Each circle represents data from one patient. Regression lines and Pearson correlations with correlation coefficients ($r$) and $p$ values are indicated.

deflections compared to non-PSD patients (Fig. 1). Considering that the amplitude of TEPs reflects information on the excitability of the local underlying cortical networks, and is sensitive to state changes (Massimini et al., 2005), the decreased TEP amplitude (response intensity, Fig. 2D–F) observed in the PSD group might represent a direct measure of neuronal dysfunction prior to delirium onset. Furthermore, the decrease of response intensity in PSD patients was distributed widely throughout extensive bihemispheric regions distant from the stimulated sites (cf. Fig. 2D–F), suggesting a suppressed propagation of the neuronal responses to other areas of the brain beyond local hypoexcitability at the sites of stimulation. Our study provides evidence that such a breakdown of effective connectivity might link with an abnormal brain state facilitating delirium development.

Disturbances in the organization of brain networks result in cognitive deficits and altered levels of attention and awareness (Chennu et al., 2017), which are typical core symptoms of delirium. Delirium has been hypothesized to be a disconnection syndrome (Sanders, 2011; van Dellen et al., 2014). In our study, to quantify the "network property" of TEPs, we calculated the symbolic transfer entropy and PCI$^{ST}$. Methodologically, symbolic transfer entropy measures information-theoretic causal relationship of TEPs and PCI$^{ST}$ measures the spatiotemporal dynamics of TEPs and reflects the joint presence of integration and differentiation in thalamocortical brain networks. The significantly decreased information flow and lower PCI$^{ST}$ values in PSD patients compared to non-PSD patients indicates reduced integration of TMS-evoked responses across cortical areas or a lack of differentiation of cortical responses (stereotypical activity). Therefore, both the suppressed propagation of TMS evoked responses, blocked information flow and the low PCI$^{ST}$ reflect disturbed effective network connectivity of PSD patients, which is consistent with the functional and structural network findings predisposing to delirium (Sanders, 2011; van Montfort et al., 2019).

From a structural prospective, white matter is considered as main propagation pathway of TMS-evoked signals. White matter disintegrity, which has been considered closely associated with delirium development (Hatano et al., 2013; Morandi et al., 2012a), should have significant influence on network integration (i.e., PCI$^{ST}$) evoked by TMS. This is consistent with our observed association of PCI$^{ST}$ with lesion voxels in deep white matter (Fig. 6A). Besides white matter lesion load, neurotransmitter and neuroendocrine dysregulation, inflammation, aging, oxidative stress, diurnal dysregulation, all of which have been considered as predisposing delirium risk factors, can affect the integrity of brain networks in stroke patients (Maldonado, 2013). Therefore, we speculate that a breakdown of effective brain network connectivity creates a vulnerable brain condition that lowers the threshold for transition from a normal state to a cognitive dysfunctional or unawareness state. This relation may be of particular relevance for advancing our understanding of the pathophysiology of delirium development in the first days after a stroke event.

Natural frequency reflects the predominant frequency of synchronization of neuronal firing in a brief period following the TMS pulse (Herring et al., 2015) and is presumably mediated through cortico-subcortical networks (Rosanova et al., 2009). Our study reports decreases of natural frequencies at each of the three TMS targets (DLPFC, M1 and SPL) of the stroke patients (Fig. 4), when compared to the natural frequency of healthy subjects reported in previous studies (Rosanova et al., 2009). The reduced TMS-induced oscillation frequencies are consistent with findings in sub-acute stroke patients reported in (Tscherpel et al., 2020). More importantly, we demonstrated that patients in the PSD group exhibited significantly lower natural frequencies compared to those in the non-PSD group. Together, slowing oscillations in

resting-state EEG and reduction of natural frequency in TMS-EEG might index a predisposing brain state of delirium.

In contrast to the network integration index PCI$^{ST}$, TMS-induced natural frequencies are a local-region specificity index. Each region tends to resonate at approximately its own characteristic frequency to TMS (Rosanova et al., 2009; Vallesi et al., 2021). Damage of gray matter and its cortico-subcortical connectivity would reduce the natural frequency (Fig. 6B) (Sarasso et al., 2020). Our natural frequency findings highlighted the DLPFC and SPL but not M1 in predicting risk of delirium development. Lesion studies and functional brain imaging offered clues that the prefrontal and parietal cortex, and the surrounding white matter, are correlated with delirium (Committeri et al., 2007; van Montfort et al., 2019). Prefrontal cortex has a unique role as the executive area of the brain for higher associative and integrative activities. Patients with delirium show a positive correlation between activity in the DLPFC and the posterior cingulate cortex compared to healthy controls who demonstrated inverse correlation (Choi et al., 2012). Prefrontal cortex has a 'supramodal executive status' for information processing and has wide-ranging effects on behavior and cognition, since it exhibits rich interconnectedness with cortical association areas, limbic cortex, and ascending brainstem neurotransmitter pathways. It is, therefore, not surprising that the dysfunctional prefrontal cortico-subcortical pathway, presented by reduction of natural frequency, was included as a predisposing risk of delirium. In addition to frontal regions, the parietal cortex also plays an important role in forming cortical top-down attention networks (Corbetta and Shulman, 2011). Stroke-induced impairments in the functioning of cortical attention networks have been associated with behavioral signs of delirium (He et al., 2007; Karnath et al., 2001). Furthermore, the dorsal and ventral parietal cortices project to and modulate the Ascending Reticular Activating System (ARAS), a system which initiates and maintains wakefulness and arousal. The ARAS was proposed a specific brain network associated with delirium (Boukrina and Barrett, 2017). The delirious patients had an acute reversible disruption of connectivity in ARAS and returned to normal after resolution of delirium (Choi et al., 2012). Therefore, functioning of the parietal cortex, participating in the top-down attention network and bottom-up (afferent) projections of ARAS, should be closely related to the neuronal mechanisms of delirium. Consistently, strokes patients with lesions at posterior parietal cortex present with severe delirium as the main clinical manifestation (Boukrina et al., 2021; Naidech et al., 2016).

Stroke lesion size (Fig. 5A), affected hemisphere, and stroke severity (Fig. 5D) have been considered risk factors for delirium (Kostalova et al., 2012; Ojagbemi et al., 2017; Pasinska et al., 2018). Although the PCI$^{ST}$ values showed inverse correlations with lesion size (Fig. 5B–C) and NIHSS (Fig. 5E–F), the covariate analyses and the stepwise logistic regression analysis including Wald statistic verified that PCI$^{ST}$ was independently associated with PSD, irrespective of lesion size, affected hemisphere or stroke severity.

Importantly, measures of cortical reactivity were significantly related to delirium duration. Lower complexity and slower TMS-induced oscillations (maximum values across the three TMS targets) were associated with longer time staying in the delirium state (Fig. 6D-E). Considering the impact of whiter matter integrity on complexity and natural frequency of TMS-evoked neural activity, these findings are in line with previous results that longer delirium duration correlated with decreased white matter integrity (Morandi et al., 2012b).

A further aim of the present study was to establish a novel approach to predict delirium risk in acute stroke patients. Although the number of studies is still limited, TMS-EEG has been shown a potentially useful technique to identify neurophysiological changes after stroke (Casula et al., 2021; Gray et al., 2017;

Pellicciari et al., 2018; Tscherpel et al., 2020). However, no TMS-EEG study so far has been applied to delirium research, probably because the technique is complex and difficult to handle at bedside.

## 4.1. Limitations

We provide first evidence that measures of cortical reactivity calculated from TMS-EEG data could be used as potential biomarkers for predicting delirium risk, but our work is not without limitations. First, although we included a representative sample of the stroke patients, the sample size is small. Therefore, the findings will have to be validated in a larger sample. Second, we used earplugs rather than noise masking as pilot testing proved auditory masking to be stressful in acute stroke patients. Further, we wanted to avoid exposure of patients to an additional risk factor for delirium. However, as we have indicated earlier, we conducted more extensive analyses compared to previous studies (Tscherpel et al., 2020; Vallesi et al., 2021) to render a major confound of our findings by auditory evoked potentials unlikely. Finally, patients without detectable MEPs were excluded from the study. Such patients could be recruited into future studies with advanced navigation systems that allow estimation of the induced electric field for determining individual TMS intensity (Sarasso et al., 2020).

## 4.2. Conclusions

EEG responses to TMS can unravel brain network states of reduced excitability, effective connectivity, complexity and natural frequency that identify acute stroke patients at high risk for development of delirium. Findings provide novel insight into the pathophysiology of pre-delirium brain states, and may promote targeted effective delirium prevention strategies in those patients at high risk. Moreover, TMS-EEG is a relatively demanding technology that cannot be easily broadly applied. Given the increasing clinical interest in TMS-EEG, we expect that this will drive technical development and simplification to make this important technology more widely available soon.

## Declaration of competing interest

The authors declare that they have no known competing financial interests or personal relationships that could have appeared to influence the work reported in this paper.

## CRediT authorship contribution statement

**Yang Bai:** Conceptualization, Data curation, Investigation, Formal analysis, Writing – original draft. **Paolo Belardinelli:** Formal analysis, Writing – review & editing. **Catrina Thoennes:** Investigation, Writing – review & editing. **Corinna Blum:** Investigation, Writing – review & editing. **David Baur:** Investigation, Writing – review & editing. **Kornelia Laichinger:** Investigation, Writing – review & editing. **Tobias Lindig:** Formal analysis, Writing – review & editing. **Ulf Ziemann:** Conceptualization, Formal analysis, Writing – review & editing. **Annerose Mengel:** Conceptualization, Formal analysis, Writing – review & editing.

## Acknowledgements

## Appendix A. Supplementary material

Supplementary data to this article can be found online at https://doi.org/10.1016/j.clinph.2022.11.017.

## References

American Psychiatric Association. Diagnostic and Statistical Manual of Mental Disorders, 5th Edition: DSM-5. United States: American Psychiatric Association; 2013.

Boukrina O, Barrett AM. Disruption of the ascending arousal system and cortical attention networks in post-stroke delirium and spatial neglect. Neurosci Biobehav Rev 2017;83:1–10.

Boukrina O, Kowalczyk M, Koush Y, Kong Y, Barrett AM. Brain Network Dysfunction in Poststroke Delirium and Spatial Neglect: An fMRI Study. Stroke 2021. STROKEAHA121035733.

Caeiro L, Ferro J, Albuquerque R, Figueira ML. Denial in the first days of acute stroke. J Neurol 2004;251:171–8.

Casali AG, Gosseries O, Rosanova M, Boly M, Sarasso S, Casali KR, et al. A theoretically based index of consciousness independent of sensory processing and behavior. Sci Transl Med 2013;5:198ra105.

Casula EP, Pellicciari MC, Bonnì S, Spanò B, Ponzo V, Salsano I, et al. Evidence for interhemispheric imbalance in stroke patients as revealed by combining transcranial magnetic stimulation and electroencephalography. Hum Brain Mapp 2021;42:1343–58.

Chennu S, Annen J, Wannez S, Thibaut A, Chatelle C, Cassol H, et al. Brain networks predict metabolism, diagnosis and prognosis at the bedside in disorders of consciousness. Brain 2017;140:2120–32.

Choi SH, Lee H, Chung TS, Park KM, Jung YC, Kim SI, et al. Neural network functional connectivity during and after an episode of delirium. Am J Psychiatry 2012;169:498–507.

Cohen MX, Donner TH. Midfrontal conflict-related theta-band power reflects neural oscillations that predict behavior. J Neurophysiol 2013;110:2752–63.

Committeri G, Pitzalis S, Galati G, Patria F, Pelle G, Sabatini U, et al. Neural bases of personal and extrapersonal neglect in humans. Brain 2007;130:431–41.

Comolatti R, Pigorini A, Casarotto S, Fecchio M, Faria G, Sarasso S, et al. A fast and general method to empirically estimate the complexity of brain responses to transcranial and intracranial stimulations. Brain Stimul 2019;12:1280–9.

Corbetta M, Shulman GL. Spatial neglect and attention networks. Annu Rev Neurosci 2011;34:569–99.

Dahl MH, Ronning OM, Thommessen B. Delirium in acute stroke–prevalence and risk factors. Acta Neurol Scand Suppl 2010;122:39–43.

Fan L, Li H, Zhuo J, Zhang Y, Wang J, Chen L, et al. The Human Brainnetome Atlas: A New Brain Atlas Based on Connectional Architecture. Cereb Cortex 2016;26:3508–26.

Gascoyne L, Furlong PL, Hillebrand A, Worthen SF, Witton C. Localising the auditory N1m with event-related beamformers: localisation accuracy following bilateral and unilateral stimulation. Sci Rep 2016;6:31052.

Godey B, Schwartz D, de Graaf JB, Chauvel P, Liegeois-Chauvel C. Neuromagnetic source localization of auditory evoked fields and intracerebral evoked potentials: a comparison of data in the same patients. Clin Neurophysiol 2001;112:1850–9.

Gosseries O, Sarasso S, Casarotto S, Boly M, Schnakers C, Napolitani M, et al. On the cerebral origin of EEG responses to TMS: insights from severe cortical lesions. Brain Stimul 2015;8:142–9.

Gray WA, Palmer JA, Wolf SL, Borich MR. Abnormal EEG Responses to TMS During the Cortical Silent Period Are Associated With Hand Function in Chronic Stroke. Neurorehabil Neural Repair 2017;31:666–76.

Gustafson Y, Olsson T, Eriksson S, Asplund K, Bucht G. Acute Confusional States (Delirium) in Stroke Patients. Cerebrovasc Dis 1991.

Hatano Y, Narumoto J, Shibata K, Matsuoka T, Taniguchi S, Hata Y, et al. White-matter hyperintensities predict delirium after cardiac surgery. Am J Geriatr Psychiatry 2013;21:938–45.

He BJ, Snyder AZ, Vincent JL, Epstein A, Shulman GL, Corbetta M. Breakdown of functional connectivity in frontoparietal networks underlies behavioral deficits in spatial neglect. Neuron 2007;53:905–18.

Herring JD, Thut G, Jensen O, Bergmann TO. Attention Modulates TMS-Locked Alpha Oscillations in the Visual Cortex. J Neurosci 2015;35:14435–47.

Hill AT, Rogasch NC, Fitzgerald PB, Hoy KE. TMS-EEG: A window into the neurophysiological effects of transcranial electrical stimulation in non-motor brain regions. Neurosci Biobehav Rev 2016;64:175–84.

Hshieh TT, Fong TG, Marcantonio ER, Inouye SK. Cholinergic deficiency hypothesis in delirium: a synthesis of current evidence. J Gerontol A Biol Sci Med Sci 2008;63:764–72.

Inouye SK, Rushing JT, Foreman M, Palmer RM, Pompei P. Does delirium contribute to poor hospital outcomes? A three-site epidemiologic study. J Gen Intern Med 1998;13:234–42.

Inouye SK, Westendorp RG, Saczynski JS. Delirium in elderly people. Lancet 2014;383:911–22.

Kalish VB, Gillham JE, Unwin BK. Delirium in older persons: evaluation and management. Am Fam Physician 2014;90:150–8.

Karnath HO, Ferber S, Himmelbach M. Spatial awareness is a function of the temporal not the posterior parietal lobe. Nature 2001;411:950–3.

Khan BA, Zawahiri M, Campbell NL, Fox GC, Weinstein EJ, Nazir A, et al. Delirium in hospitalized patients: implications of current evidence on clinical practice and future avenues for research–a systematic evidence review. J Hosp Med 2012;7:580–9.

Kiely DK, Marcantonio ER, Inouye SK, Shaffer ML, Bergmann MA, Yang FM, et al. Persistent delirium predicts greater mortality. J Am Geriatr Soc 2009;57:55–61.

Kostalova M, Bednarik J, Mitasova A, Dusek L, Michalcakova R, Kerkovsky M, et al. Towards a predictive model for post-stroke delirium. Brain Inj 2012;26:962–71.

Langhorne P, Stott DJ, Robertson L, Macdonald J, Jones L, Mcalpine C, et al. Medical complications after stoke : a multicenter study. Stroke 2000;31:1223–9.

Leslie DL, Marcantonio ER, Zhang Y, Leo-Summers L, Inouye SK. One-year health care costs associated with delirium in the elderly population. Arch Intern Med 2008;168:27–32.

Maldonado JR. Neuropathogenesis of delirium: review of current etiologic theories and common pathways. Am J Geriatr Psychiatry 2013;21:1190–222.

Massimini M, Ferrarelli F, Huber R, Esser SK, Singh H, Tononi G. Breakdown of cortical effective connectivity during sleep. Science 2005;309:2228–32.

McCusker J, Cole M, Abrahamowicz M, Primeau F, Belzile E. Delirium predicts 12-month mortality. Arch Intern Med 2002;162:457–63.

McManus J, Pathansali R, Hassan H, Ouldred E, Cooper D, Stewart R, et al. The course of delirium in acute stroke. Age Ageing 2009;38:385–9.

Morandi A, Rogers BP, Gunther ML, Merkle K, Pandharipande P, Girard TD, et al. The relationship between delirium duration, white matter integrity, and cognitive impairment in intensive care unit survivors as determined by diffusion tensor imaging. Crit Care Med 2012a;40:2182.

Morandi A, Rogers BP, Gunther ML, Merkle K, Pandharipande P, Girard TD, et al. The relationship between delirium duration, white matter integrity, and cognitive impairment in intensive care unit survivors as determined by diffusion tensor imaging: the VISIONS prospective cohort magnetic resonance imaging study*. Crit Care Med 2012b;40:2182.

Naidech AM, Polnaszek KL, Berman MD, Voss JL. Hematoma Locations Predicting Delirium Symptoms After Intracerebral Hemorrhage. Neurocrit Care 2016;24:397–403.

Ojagbemi A, Owolabi M, Bello T, Baiyewu O. Stroke severity predicts poststroke delirium and its association with dementia: Longitudinal observation from a low income setting. J Neurol Sci 2017;375:376–81.

Oldenbeuving AW, Kort P, Jansen B, Roks G, Kappelle LJ. Delirium in acute stroke: a review. Int J Stroke 2007;2.

Oldenbeuving AW, Kort PD, Jansen B, Algra A, Kappelle LJ, Roks G. Delirium in the acute phase after stroke: incidence, risk factors, and outcome. Neurology 2013;76:993–9.

Pasinska P, Kowalska K, Klimiec E, Szyper-Maciejowska A, Wilk A, Klimkowicz-Mrowiec A. Frequency and predictors of post-stroke delirium in PRospective Observational POLish Study (PROPOLIS). J Neurol 2018;265:863–70.

Pellicciari MC, Bonni S, Ponzo V, Cinnera AM, Mancini M, Casula EP, et al. Dynamic reorganization of TMS-evoked activity in subcortical stroke patients. Neuroimage 2018;175:365–78.

Premoli I, Bergmann TO, Fecchio M, Rosanova M, Biondi A, Belardinelli P, et al. The impact of GABAergic drugs on TMS-induced brain oscillations in human motor cortex. Neuroimage 2017;163:1–12.

Rice KL, Bennett MJ, Berger L, Jennings B, Eckhardt L, Fabré-LaCoste N, et al. A pilot randomized controlled trial of the feasibility of a multicomponent delirium prevention intervention versus usual care in acute stroke. J Cardiovasc Nurs 2017;32:E1–E10.

Rocchi L, Di Santo A, Brown K, Ibáñez J, Casula E, Rawji V, et al. Disentangling EEG responses to TMS due to cortical and peripheral activations. Brain Stimul 2021;14:4–18.

Rogasch NC, Thomson RH, Farzan F, Fitzgibbon BM, Bailey NW, Hernandez-Pavon JC, et al. Removing artefacts from TMS-EEG recordings using independent component analysis: importance for assessing prefrontal and motor cortex network properties. Neuroimage 2014;101:425–39.

Rosanova M, Casali A, Bellina V, Resta F, Mariotti M, Massimini M. Natural frequencies of human corticothalamic circuits. J Neurosci 2009;29:7679–85.

Sanders RD. Hypothesis for the pathophysiology of delirium: role of baseline brain network connectivity and changes in inhibitory tone. Med Hypotheses 2011;77:140–3.

Sarasso S, D'Ambrosio S, Fecchio M, Casarotto S, Vigano A, Landi C, et al. Local sleep-like cortical reactivity in the awake brain after focal injury. Brain 2020;143:3672–84.

Saturnino GB, Puonti O, Nielsen JD, Antonenko D, Madsen KH, Thielscher A. SimNIBS 2.1: a comprehensive pipeline for individualized electric field modelling for transcranial brain stimulation. In: Makarov S, Horner M, Noetscher G, editors. Brain and human body modeling: computational human modeling at EMBC 2018, Cham (CH); 2019. p. 3–25.

Sekihara K, Nagarajan SS. Adaptive spatial filters for electromagnetic brain imaging. Springer Science & Business Media; 2008.

Shafi MM, Santarnecchi E, Fong TG, Jones RN, Marcantonio ER, Pascual-Leone A, et al. Advancing the Neurophysiological Understanding of Delirium. J Am Geriatr Soc 2017;65:1114–8.

Shaw RC, Walker G, Elliott E, Quinn TJ. Occurrence Rate of Delirium in Acute Stroke Settings: Systematic Review and Meta-Analysis. Stroke 2019;50:3028–36.

Siddiq N, House AO, Holmes JD. Occurrence and outcome of delirium in medical in-patients: a systematic literature review. Age Ageing 2006;35:350–64.

Song J, Lee M, Jung D. The effects of delirium prevention guidelines on elderly stroke patients. Clin Nurs Res 2018;27:967–83.

Tremblay S, Rogasch NC, Premoli I, Blumberger DM, Casarotto S, Chen R, et al. Clinical utility and prospective of TMS-EEG. Clin Neurophysiol 2019;130:802–44.

Tscherpel C, Dern S, Hensel L, Ziemann U, Fink GR, Grefkes C. Brain responsivity provides an individual readout for motor recovery after stroke. Brain 2020;143:1873–88.

Vallesi A, Del Felice A, Capizzi M, Tafuro A, Formaggio E, Bisiacchi P, et al. Natural oscillation frequencies in the two lateral prefrontal cortices induced by Transcranial Magnetic Stimulation. Neuroimage 2021;227 117655.

van Dellen E, van der Kooi AW, Numan T, Koek HL, Klijn FA, Buijsrogge MP, et al. Decreased functional connectivity and disturbed directionality of information flow in the electroencephalography of intensive care unit patients with delirium after cardiac surgery. Anesthesiology 2014;121:328–35.

van den Boogaard M, Schoonhoven L, Maseda E, Plowright C, Jones C, Luetz A, et al. Recalibration of the delirium prediction model for ICU patients (PRE-DELIRIC): a multinational observational study. Intensive Care Med 2014;40:361–9.

van Montfort SJT, van Dellen E, Stam CJ, Ahmad AH, Mentink LJ, Kraan CW, et al. Brain network disintegration as a final common pathway for delirium: a systematic review and qualitative meta-analysis. Neuroimage Clin 2019;23 101809.

van Munster BC, de Rooij S, Yazdanpanah M, Tienari PJ, Pitkala KH, Osse RJ, et al. The association of the dopamine transporter gene and the dopamine receptor 2 gene with delirium, a meta-analysis. Am J Med Genet B Neuropsychiatr Genet 2010;153B:648–55.

Wassenaar A, van den Boogaard M, van Achterberg T, Slooter AJ, Kuiper MA, Hoogendoorn ME, et al. Multinational development and validation of an early prediction model for delirium in ICU patients. Intensive Care Med 2015;41:1048–56.

Wiegand TLT, Remi J, Dimitriadis K. Electroencephalography in delirium assessment: a scoping review. BMC Neurol 2022;22:86.

Ye S, Kitajo K, Kitano K. Information-theoretic approach to detect directional information flow in EEG signals induced by TMS. Neurosci Res 2020;156:197–205.